



Inhibition of CO₂ corrosion of carbon steel with 1% Cr

L.D. Paolinelli^{a,*}, B. Brown^b, S.N. Simison^a, S. Nescic^b

^a Corrosion Division, INTEMA-CONICET, University of Mar del Plata, Juan B. Justo 4302 (B7608FDQ), Argentina

^b Institute for Corrosion and Multiphase Technology, Ohio University, Athens, OH 45701, USA

HIGHLIGHTS

- ▶ The imidazoline-based inhibitor used has a lower performance on carbon steel with 1% Cr.
- ▶ Inhibitor adsorption kinetics were enhanced with the increase of rotation rate.
- ▶ Fluid flow velocity may be an important parameter for the inhibition of carbon steel with 1% Cr.
- ▶ Effective inhibition of carbon steel with 1% Cr was achieved only at higher rotation rates.
- ▶ Localized corrosion was found for carbon steel with 1% Cr inhibited at the lower rotation rate.

ARTICLE INFO

Article history:

Received 24 November 2011

Received in revised form

13 June 2012

Accepted 23 August 2012

Keywords:

Corrosion

Alloys

Electrochemical techniques

SEM

ABSTRACT

One of the most employed methods for CO₂ corrosion control in oil and gas production and transportation industry is the use of carbon and low alloy steels in conjunction with corrosion inhibitors. The inhibitor performance can be influenced by the microstructure and chemical composition of the steel. In previous works, it was shown that 1% Cr addition to carbon steel decreased the protectiveness of a commercial imidazoline-based inhibitor. However, it was suspected that changing the flow rates may modify the inhibitor behaviour. In the present work, the performance of an imidazoline-based inhibitor was investigated on two carbon steels one with the other without 1% Cr, under different flow rates.

Corrosion and corrosion inhibition experiments were carried out using a rotating cylinder electrode at different rotation speeds in a deoxygenated 5 wt.% NaCl CO₂-saturated solution at 40 °C, pH 6 with and without inhibitor addition. Electrochemical measurements were taken during each experiment and sample surfaces were analyzed after each experiment. Inhibitor performance was found to be dependent on flow velocity and chemical composition of carbon steel.

© 2012 Elsevier B.V. All rights reserved.

1. Introduction

Little is known regarding CO₂ corrosion inhibition of Cr-containing carbon steels. It has been reported that steels alloyed with small Cr contents (0.5–1%) are less efficiently inhibited than Cr-free carbon steels [1–4]. However, other authors tested various inhibitors on carbon steels with and without 0.5% Cr and found that all the employed compounds achieved acceptable efficiencies on both steels [5]. Recently, it has been shown that the addition of 1% Cr in carbon steel has a negative effect on the adsorption of a commercial imidazoline-based inhibitor, leading to localized corrosion, more or less severe, depending on steel microstructure and pre-corrosion period [6]. It needs to be noted that the latter set of results were obtained under low flow rate (glass cells with low

speed magnetic stirring), thus experimentation under more representative hydrodynamic conditions would be valuable.

It is known that CO₂ corrosion can be influenced by the hydrodynamic conditions, due to changes in transport of reactive species to surface and differences in the formation and destruction of protective corrosion product layers. The main way to characterize the intensity of the flow is the wall shear stresses [7,8]. Additionally, it has long been suspected that corrosion inhibitors performance can be also affected by the flow regime (in multiphase flow) and flow velocity. For single phase flow, it has been reported that low fluid velocities or stagnant conditions produce an enhancement of protective properties of the inhibitor films [9]. This beneficial effect would be related to smaller flow-induced shear stresses applied on the inhibitor film and the decrease in the availability of corrosive species given by a lower mass transfer rate. Nevertheless, other researchers have found that inhibitors performance or inhibitor protective films are not affected by wall shear stresses for the range of flow velocities usually used in service [10,11].

* Corresponding author. Tel.: +54 223 4816600x247; fax: +54 223 4810046.
E-mail address: lpaolinelli@f.mdp.edu.ar (L.D. Paolinelli).

Table 1
Chemical composition of the tested materials (major alloying elements).

Materials	(% wt.) Fe balance			
	C	Mn	Si	Cr
C–Mn	0.38	0.99	0.33	0.17
1Cr	0.39	1.01	0.26	1.02

One of the most cost-effective and therefore most employed methods for CO₂ corrosion control in oil and gas production and transportation industry is the use of carbon and low alloy steels in conjunction with corrosion inhibitors [12]. Organic substances containing nitrogen have been successfully applied for CO₂ corrosion inhibition of carbon steel. Especially, corrosion inhibitors based on amides derivatives, such as imidazolines (e.g. oleic imidazoline) are extensively used to protect carbon steel tubes and pipes [9].

Steel metallurgy has also been employed as a method of corrosion control for CO₂ corrosion. A positive contribution of low Cr additions (up to 5%) to the corrosion resistance of standard carbon steel has been reported [12–18]. This improvement is based on the formation of a stable protective chromium containing oxide film [17,18]. Nevertheless, some researchers have found an adverse behaviour particularly for Cr contents from 0.5 to 1.5% [5,6,12,16,19].

The aim of the present work is to investigate the performance of an imidazoline-based inhibitor on two carbon steels with and without 1% Cr under different flow velocities employing a RCE (Rotating Cylinder Electrode) device.

2. Experimental

Two types of carbon steels for oil and gas production tubes were used for the electrochemical experiments. Their chemical compositions (wt.%) are listed in Table 1. A laboratory heat treatment of quenching and tempering (austenized at 890 °C, water quenching and 1 h tempering at 700 °C) was performed on both steels in order

to obtain the same microstructure with globular cementite morphology (Fig. 1).

Working electrodes were machined from these heat-treated materials into 10 mm diameter cylinders with a total exposed area of 4.2 cm². For the electrochemical test, surfaces were polished to 600-grit SiC paper, washed with distilled water and rinsed and maintained in acetone until the immersion procedure.

Experiments were conducted at open circuit potential using a rotating cylinder electrode. The rotation speeds were 250, 1000 and 2500 rpm, leading to peripheral flow velocities of 0.13, 0.52 and 1.3 m s⁻¹ and turbulent Reynolds numbers of 990, 3880 and 9940, respectively. A three-electrode electrochemical cell with a working volume of 2 L was used. The test media was a deoxygenated 5 wt. % NaCl (analytical-reagent grade) solution saturated with CO₂, 40 °C, atmospheric pressure and pH 6 adjusted adding deoxygenated 1 M NaHCO₃ solution. Positive CO₂ pressure was maintained throughout the experiments to avoid air ingress. The reference electrode was Ag/AgCl and the counter electrode was a platinum wire. Fig. 2 depicts a scheme of the test electrochemical cell employed and its accessories.

Prior to electrode immersion, a commercial imidazoline-based inhibitor was added in a concentration recommended by manufacturer – 50 ppm. A schematic representation of the imidazoline molecule is shown in Fig. 3. Inhibitor performance was monitored after 1, 1.5, 2 and 24 h by means of electrochemical techniques: corrosion potential (E_{corr}), polarization resistance (LPR) and electrochemical impedance spectroscopy (EIS), employing a Gamry[®] CMS100 potentiostat.

LPR experiments were done by polarizing the working electrode ± 0.01 V versus E_{corr} with a sweep rate of 10^{-4} V s⁻¹. EIS was measured at E_{corr} using an applied potential of ± 0.005 V rms with a frequency interval of 60,000 to 0.003 Hz. E_{corr} was monitored before each DC and AC analyses. The electrochemical data were analyzed using Gamry[®] software and Zview 2[®] software. Corrosion rates (CR) were calculated with polarization resistance (Rp) values obtained from LPR measurements, using the Stern–Geary equation with a proportionality factor $B = 0.022$ V [6].

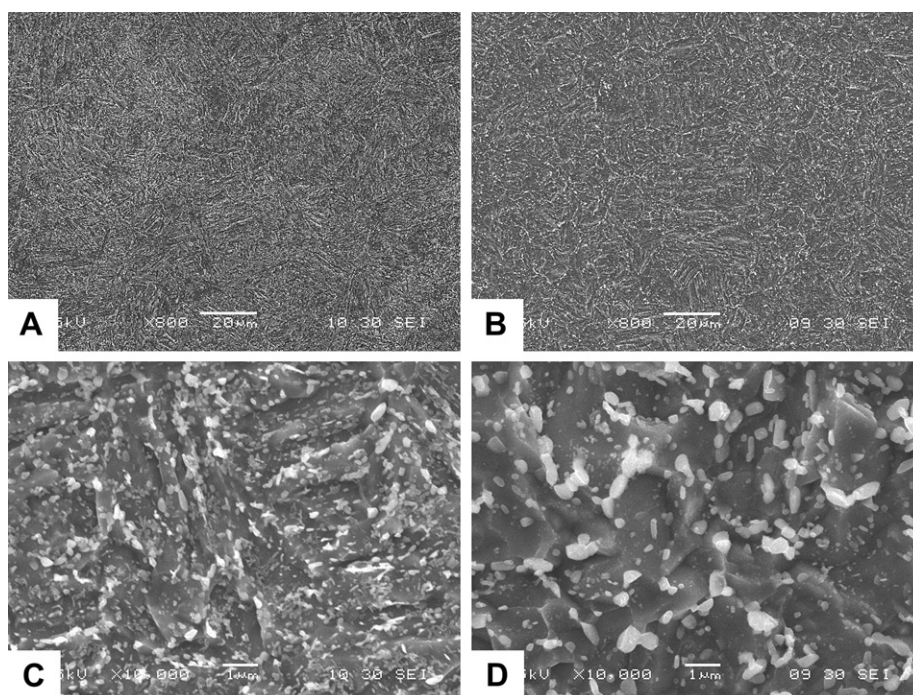


Fig. 1. Steel microstructure: A) 1Cr, B) C–Mn. High magnification: C) 1Cr, D) C–Mn. Nital etching.

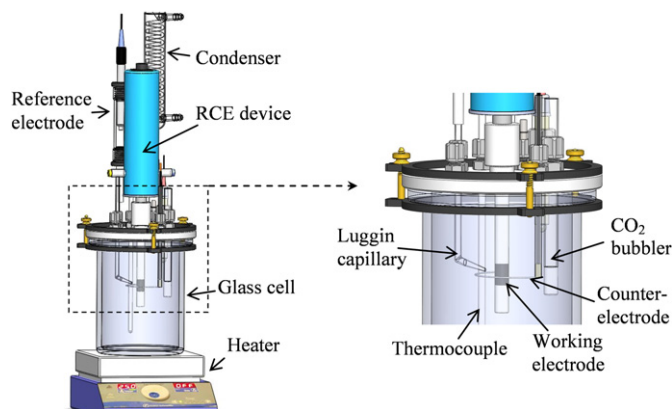


Fig. 2. Schematic representation of the test electrochemical cell.

To characterize the inhibited surfaces, a scanning electron microscope JEOL[®] JSM-6390 with EDS was used. The assessment of corroded zones in the tested samples was accomplished from SEM images using Image-Pro Plus[®] software for area quantification. Corrosion products were then chemically/mechanically removed [20] and damage profiles were obtained with an Alicona[®] infinite focus microscope (IFM) to measure the penetration of the corrosion attack.

3. Results

3.1. D.C. electrochemical results

Fig. 4 shows R_p and E_{corr} values within the first 2 h of inhibition for C–Mn and 1Cr samples. R_p values can be used to understand the adsorption kinetics of the inhibitor, since for short times of exposure the increase of R_p value is directly related to the surface coverage. Without inhibitor addition, R_p values of all tested samples are practically independent of rotation speed. This behaviour was also observed for $\text{pH} > 5$ in another study [7]. It is worth noting that R_p values of both steels immersed without inhibitor are stable and E_{corr} values vary less than 20 mV along the period tested.

When samples are exposed to inhibitor, a rapid rise of R_p for both steels occurs, particularly for the highest rotation speeds of 1000 and 2500 rpm. It is worth noting that C–Mn samples show better inhibition (surface coverage) than 1Cr samples for all the tested rotation speeds. E_{corr} of the inhibited steels shifts to more positive values throughout immersion time, indicating that this kind of inhibitor acts more efficiently on the anodic reaction. Polarization curves of C–Mn steel treated with this kind of inhibitor can be found elsewhere [21].

Fig. 5 shows the corrosion rates of C–Mn and 1Cr samples for different rotation speeds and inhibition times. It can be seen that C–Mn samples present a decrease in corrosion rates of at least 2

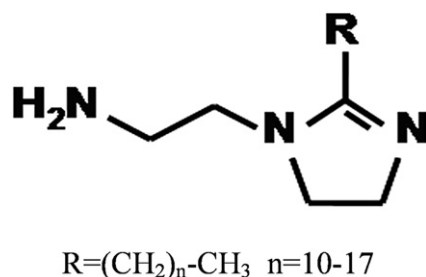


Fig. 3. Schematic representation of an imidazoline molecule.

orders of magnitude at the end of inhibition period (24 h) for all the tested flow velocities. For 1Cr samples, a decrease of corrosion rates is also seen, but it is less pronounced than in C–Mn samples. It should be noted that within the first 24 h, higher rotation speeds resulted in lower corrosion rates for all exposure times.

Table 2 lists inhibitor efficiency values of C–Mn and 1Cr steels (calculated by Eq. (1)) for different inhibition times and rotation speeds.

$$\eta = \left(1 - \frac{R_p}{R_p'}\right) \cdot 100 \quad (1)$$

where: η : inhibitor efficiency (%), R_p : polarization resistance measured without the inhibitor, R_p' : polarization resistance measured with the inhibitor added.

The calculated inhibitor efficiencies approach 100% on both steels from 1 h of exposure for the highest rotation speeds (1000 and 2500 rpm). In the case of the lowest rotation speed, the efficiencies result lower particularly on 1Cr samples; however they come close to 100% after 24 h. It is worth noting that the differences on the inhibitor performance found between C–Mn and 1Cr samples (for example, almost one order of magnitude in R_p values for the inhibition at 2500 rpm) are overlooked by the efficiency calculations. This is due to the asymptotic nature of the efficiency function (Eq. (1)).

Efficiency calculations are always based on the assumption that the rate of attack is uniform. Users select inhibitors based on efficiencies values calculated this way. Moreover, in most of the publications in literature no evidence of surface attack is given or commented. However, as will be shown in the following section, if localized corrosion is present, efficiency values are not indicative of the actual corrosion rate, then an examination of exposed surfaces is needed.

3.2. Surface analysis

From surface inspection (SEM and IFM analysis), it was determined that the corrosive attack of all samples of both steels tested without inhibitor at different flow rates was uniform.

For all evaluated flow rates, inhibited surfaces of C–Mn steel remain practically intact throughout the inhibition period since original polishing marks are clearly distinguished. As an example, SEM images of C–Mn samples inhibited for 24 h at 250 rpm are shown in Fig. 6.

In the case of 1Cr samples, different surface morphologies can be found according to flow rates. For 250 rpm, the surface is not completely inhibited (Fig. 7) as shown by zones where the inhibitor acted less efficiently and corrosion kept progressing (Fig. 7C). These regions present corrosion products with Cr enrichment up to 12 wt. % (EDS measurement), while on protected zones (Fig. 7E) the surface Cr content is similar to the freshly polished steel surface. A similar pattern of attack can be found on samples inhibited at 1000 rpm (Fig. 8), but in this case, the affected area is smaller and the attack is less severe than on samples tested at 250 rpm. The affected zones show lower Cr contents of around 7 wt. %. The nature of the chromium-rich corrosion products found in the corroded surfaces of 1Cr steel is discussed elsewhere [6]. The surface of samples inhibited at 2500 rpm (Fig. 9) is almost intact as was the case of inhibited C–Mn samples.

From SEM and IFM analyses (Fig. 10) of 1Cr coupons inhibited for 24 h at 250 rpm it was determined an affected area of around 2.5% and a maximum depth of attack of 14 μm . Therefore, it can be inferred that affected zones suffer corrosion rates as high as 5 mm y^{-1} , almost 3 times higher than the uninhibited corrosion rate ($\sim 2 \text{ mm y}^{-1}$). Samples tested at 1000 rpm present a ratio of

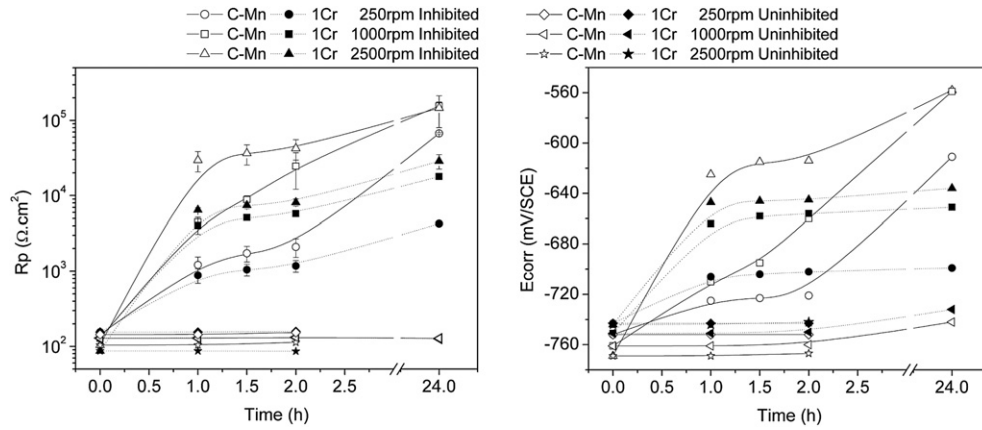


Fig. 4. Rp and E_{corr} versus immersion time for inhibited and uninhibited C–Mn and 1Cr steels.

affected area of about 0.03% and a maximum depth of damage of 6 μm. In this case maximum estimated corrosion rate of affected zones is similar to the uninhibited measured one.

3.3. EIS results

Fig. 11 shows impedance spectra of C–Mn and 1Cr samples inhibited at different rotation speeds. Uninhibited samples response was added as a reference.

For samples exposed without inhibitor addition, only one time constant is distinguishable in the phase angle (α) versus frequency (f) plot. This time constant is related to the corrosion processes at the metal/electrolyte interface and can be modelled by a Randles equivalent circuit that allows charge transfer resistance (R_{CT}), electrolyte resistance (R_S) and double layer capacitance calculation. For best fitting of experimental data, the Randles circuit was modified replacing the ideal capacitor by a constant phase element (CPE) as is shown in Fig. 12a as Z_{CPEdl}. The impedance of a CPE can be expressed as:

$$Z_{CPE} = Y^{-1}(i\omega)^{-n} \tag{2}$$

where: Y is proportional to the capacitance of the interface [22], i is √−1, and n represents a phase shift.

After 2 h of exposure to an inhibited solution, at least two time constants can be detected from α versus f plot for both steels. The high frequency time constant would indicate the presence of a protective and isolating inhibitor film, while the low frequency time constant could be related to corrosion processes at the sites of metal surface uncovered by the inhibitor film [21,23,24]. In order to model this behaviour, the equivalent circuit illustrated in Fig. 12b was proposed. It represents a porous inhibitor film formed on metal surface, in which Z_{CPEFO} is related to the non-ideal capacitance of the inhibitor film, R_{FO} to the inhibitor film pore resistance and Z_{CPEdl} to the non-ideal capacitance of the double layer of the metal/electrolyte interface. However, experimental data shows a more complex behaviour in most of the tested conditions, especially for 24 h of inhibition. Thus, an additional circuit shown in Fig. 12c was employed for the modelling, which is in very good agreement with the experimental data. This equivalent circuit corresponds to a bilayer porous inhibitor film [21,25] where the inner layer is formed on the metal surface and the outer layer is on top of the latter, and both have different electrical properties. Z_{CPEFO} and R_{FO} and Z_{CPEFI} and R_{FI} are related to the non-ideal capacitance and to the pore resistance of the outer and inner layer of the inhibitor film, respectively.

Equivalent circuits presented in Fig. 12b and c are developed under the assumption of generalized inhibition (on whole surface), which is true for C–Mn samples inhibited at all tested rotation rates and 1Cr samples inhibited at 2500 rpm. However, for 1Cr samples inhibited at 250 and 1000 rpm, the occurrence of localized corrosion was shown (Section 3.2). In this circumstance, the use of equivalent circuits representing generalized inhibition may give erroneous estimation of the impedance parameters of the inhibitor film as well as of the metal–electrolyte charge transfer depending on the relationship between the localized corrosion current and the total corrosion current of the specimen. If the localized/total current ratio results in a small value

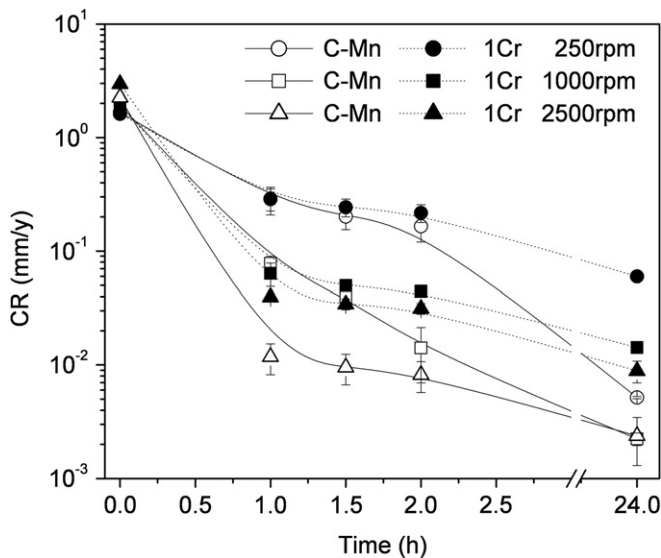


Fig. 5. Corrosion rates versus immersion time for inhibited C–Mn and Cr steels.

Table 2
Inhibitor efficiencies (η%) versus immersion time for C–Mn and 1Cr steels.

Exposure (h)	C–Mn			1Cr		
	250 rpm	1000 rpm	2500 rpm	250 rpm	1000 rpm	2500 rpm
1	88.1	97.1	99.6	82.4	96.8	98.6
1.5	91.7	98.5	99.7	85.2	97.5	98.8
2	93.1	99.5	99.7	86.8	97.7	98.9
24	99.8	99.9	99.9	96.4	99.3	99.7

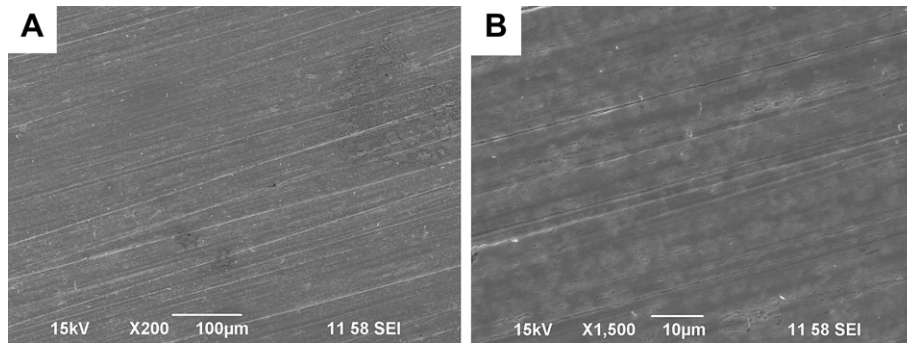


Fig. 6. Surfaces of C–Mn samples inhibited for 24 h at 250 rpm. A) and B) correspond to low and high magnification, respectively.

(e.g. less than 0.1), it means that the impedance spectrum of the specimen can be mainly attributed to the electrochemical behaviour of the inhibited surface. On the contrary, if localized/total current ratio approaches 1, the impedance spectrum can be mainly attributed to the electrochemical behaviour of the localized corrosion sites.

The former analysis was made for inhibited 1Cr samples affected by localized corrosion in order to determine the validity of employing the equivalent circuits shown in Fig. 12 for inhibitor film characterization. Total and localized corrosion currents were calculated for each inhibited specimen. The total corrosion currents of the specimens were estimated from their R_p values using Stern–

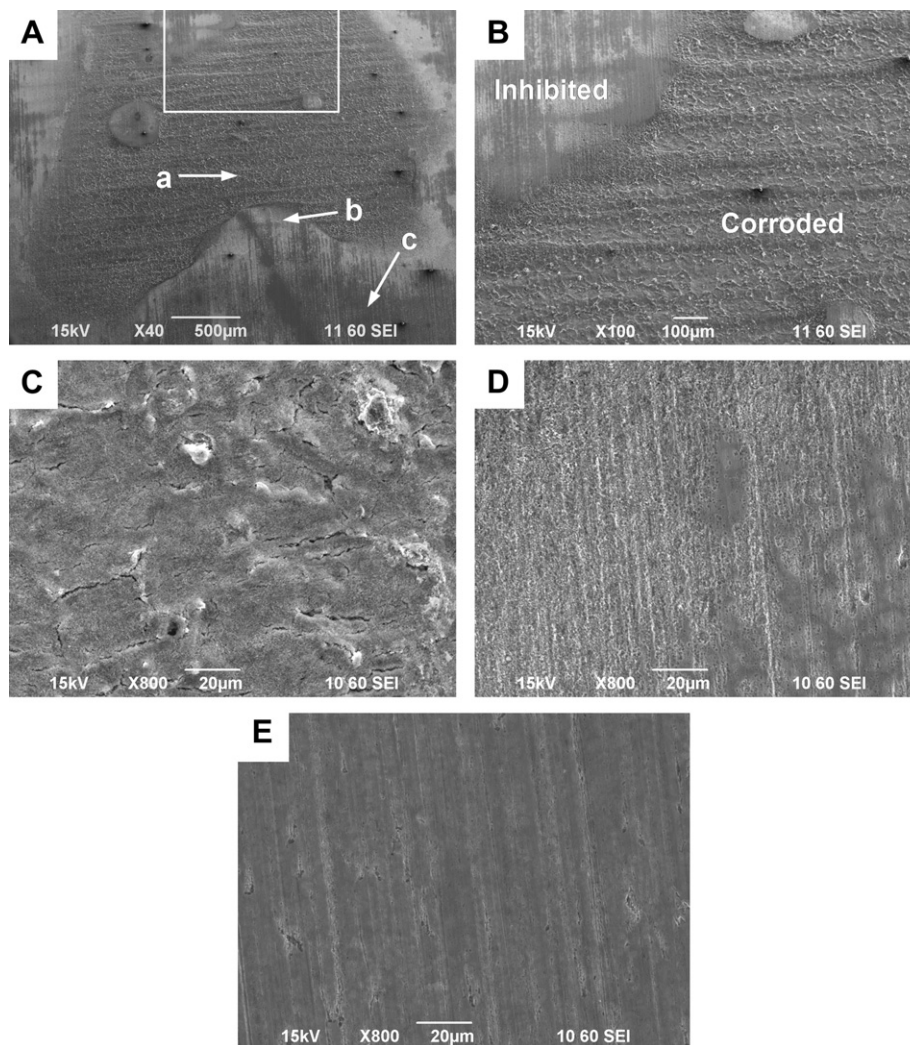


Fig. 7. Surfaces of 1Cr samples inhibited for 24 h at 250 rpm. A) General view of an uninhibited zone. B) Magnification of the border between the inhibited and the corroded zones (white rectangle in picture A). C) Corrosion products of the uninhibited zone (magnification of region (a) in picture A). D) Transition zone between the inhibited and the corroded zones (magnification of region (b) in picture A). E) Inhibited zone (magnification of region (c) in picture A).

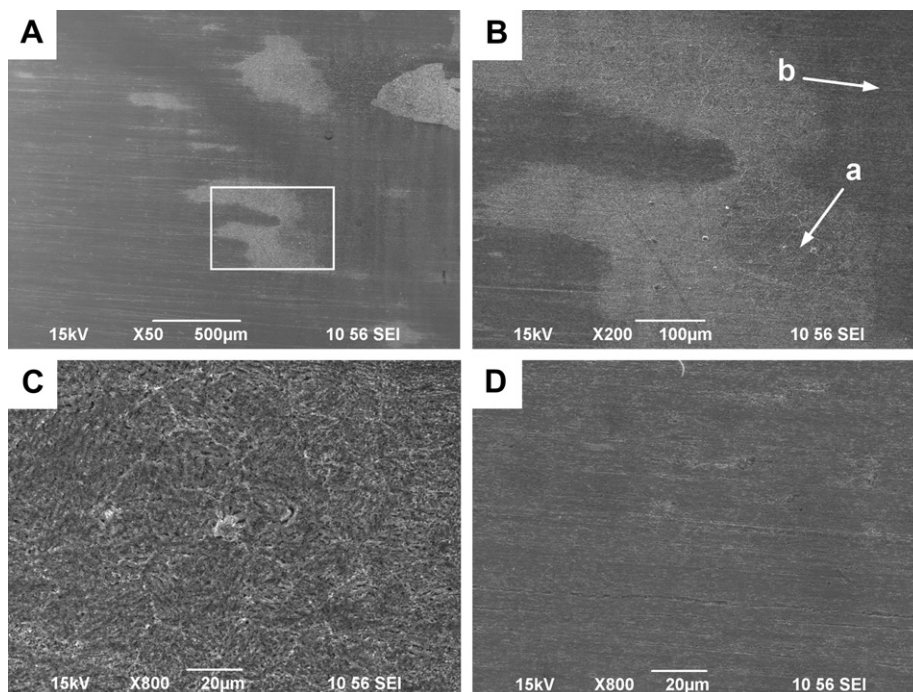


Fig. 8. Surfaces of 1Cr samples inhibited for 24 h at 1000 rpm. A) General view of an uninhibited zone. B) Magnification of an uninhibited zone (white rectangle in picture A). C) Corrosion products on an uninhibited zone (magnification of region (a) in picture B). D) Inhibited zone (magnification of region (b) in picture B).

Geary equation and their total exposed area. The localized corrosion current was conservatively estimated considering that all affected areas on the specimen were corroded at the highest possible rate, calculated from the maximum measured depth of attack. Finally, the calculated localized/total corrosion current ratios were about 1 and 0.05 for 250 and 1000 rpm, respectively.

The low value obtained for 1Cr samples inhibited at 1000 rpm allows the interpretation of impedance data under the assumption of generalized inhibition, employing the previously proposed equivalent circuits. Conversely, the impedance results from 1Cr samples inhibited at 250 rpm can not be analyzed in the same way and must be modelled with more complex circuits, taking into account the existence of localized corrosion paths in parallel to the inhibited areas. On the other hand, as localized corrosion is a random process, statistical analysis of the distribution of attack depths should be done in order to extract useful conclusions. Such analysis exceeds the scope of this paper, thus, the modelling of impedance data of 1Cr samples inhibited at 250 rpm will not be included.

Calculated circuit parameters from the modelling of impedance spectra of C–Mn and 1Cr steel are listed in Tables 3 and 4, correspondingly. The fitting and iteration errors were below 10% in each case. Fitting curves obtained from the models are plotted with solid lines on experimental data in Fig. 11.

In Fig. 11 and Tables 3 and 4, it can be observed that both steels corroded in uninhibited solution show similar frequency response and equivalent circuit parameters for all the tested rotation rates. These results are in concordance with the D.C. results previously shown.

For C–Mn steel inhibited at 250 rpm, the EIS results at the first 2 h of exposure show the existence of a porous inhibitor film. The increase in charge transfer resistance (R_{CT}) and the decrease in parameter Y_{CPEdI} due to the blocking of the exposed metal surface confirm this interpretation. Increasing the rotational speed (e.g. 1000 or 2500 rpm) enhances inhibitor film quality as shown by the formation of an inhibitor film of more complex structure with a larger film pore resistance ($R_F = R_{FO} + R_{FI}$), besides a higher R_{CT} and a lower Y_{CPEdI} parameter.

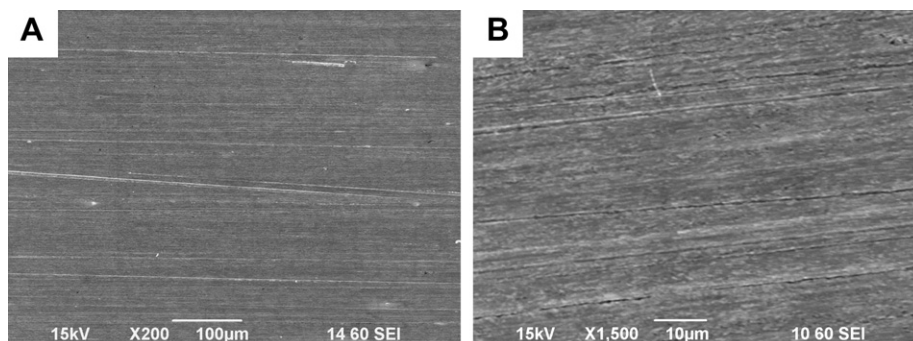


Fig. 9. Surfaces of 1Cr samples inhibited for 24 h at 2500 rpm. A) and B) correspond to low and high magnification, respectively.

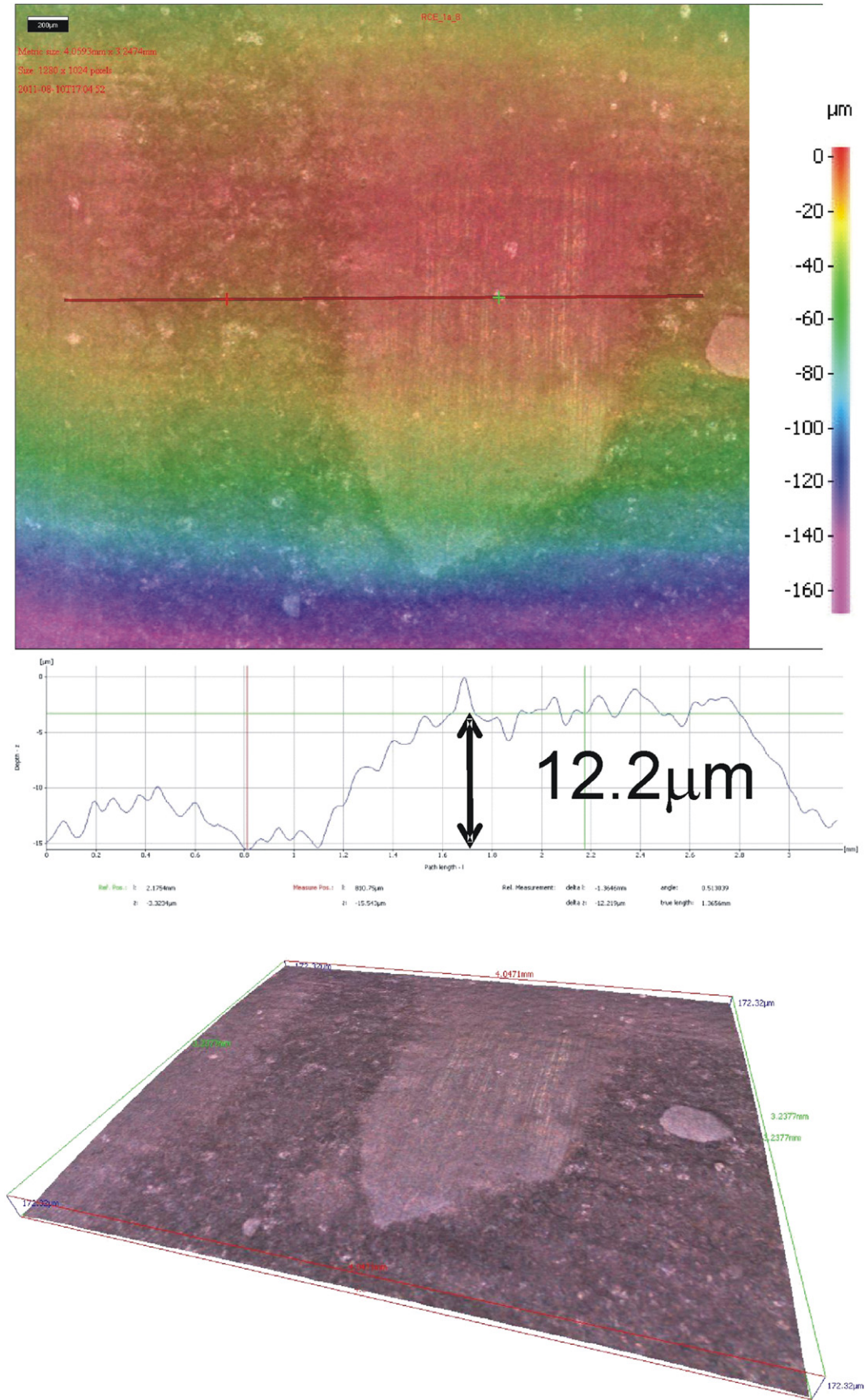


Fig. 10. Topography and cross section profile of affected areas of a 1Cr sample inhibited at 250 rpm.

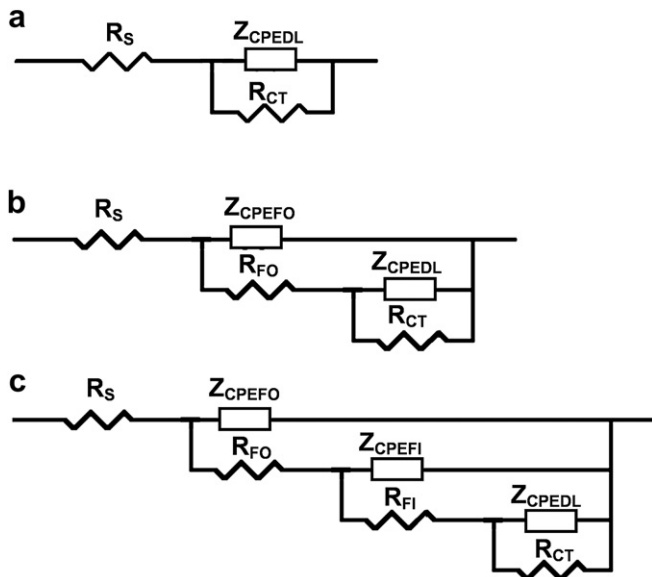


Fig. 12. Different equivalent circuits used for the modelling of impedance data.

In the case of 1Cr steel inhibited at 1000 rpm (Table 4), at the first 2 h of immersion an increase of R_{CT} and a decrease of Y_{CPEDL} can be observed due to the formation of an inhibitor film. An improvement of the inhibitor film with rotation rate is also seen, as in the case of C–Mn samples. The film pore resistance (R_{FO}) increases as well as R_{CT} , and Y_{CPEDL} decreases for rotation rates from 1000 to 2500 rpm.

Comparing the inhibitor performance on both steels at 2 h of exposure at 1000 and 2500 rpm, the inhibitor films formed on 1Cr samples are worse developed and less isolating than the ones formed on C–Mn samples, showing one layer instead two, with a lower pore resistance (R_{FO}) and a lower coverage (lower R_{CT}).

After 24 h of inhibition, all the analyzed samples show an increase of the R_{CT} and a decrease of Y_{CPEDL} , jointly with an increase of R_F (R_{FO} and R_{FI}). This behaviour points out an enhancement of the protectiveness of the inhibitor films. Moreover, at this exposure time, inhibitor films formed on both steels seem to develop the same complex structure independently of the rotation rate used, but they show better isolating properties as the rotation rate is higher (as shown at 2 h).

It is worth noting that inhibitor film resistances (R_{FI} and R_{FO}) and charge transfer resistances (R_{CT}) calculated for C–Mn steel are almost an order of magnitude greater than the corresponding parameters of 1Cr steel at the same experimental condition. This indicates that C–Mn steel shows better inhibition than 1Cr steel, which is in agreement with the D.C. results (Figs. 4 and 5).

Regarding the bilayer inhibitor film structure developed on both steels, the resistance of the inner layer (R_{FI}) is much larger than that of the outer layer (R_{FO}). This would suggest that the number of pores per unit of area and/or the size of the pores that could be penetrated by the electrolyte is smaller. This could be related to an inner layer with a higher molecular density as proposed elsewhere [21,26]. The Y_{CPEFI} parameter associated with capacitance of the inner layer is higher than the Y_{CPEFO} parameter of the outer layer, possibly due to differences in their dielectric constants and/or thicknesses. The values of the constant phase exponents: n_{CPEFI} and n_{CPEdi} are between 0.5 and 0.66. Such low values would indicate a strong heterogeneity in the current flowing through both layers and through inner layer to metal surface. This could be attributed to an unclearly defined limit between both inner and outer film layers. In addition, non-uniform mass transfer and different local surface properties may also generate time-constant dispersion [27].

4. Discussion

From the results presented above, important differences on the inhibition of carbon steel with and without 1% Cr can be observed. Although calculated inhibitor efficiencies at 24 h are over 95% for both steels in all tested conditions, 1Cr steel can suffer severe localized corrosion depending on flow velocity. The observed inhibited corrosion rates are higher for 1Cr steel than for C–Mn steel, especially at the end of inhibition period (24 h), as a result of the inferior protective properties of the formed inhibitor films.

The lower performance of the imidazoline-based inhibitor would indicate that α -Fe containing 1% Cr is not as good a substrate for inhibitor adsorption than Cr-free α -Fe, as was shown in previous work [6]. This effect would be attributed to the spontaneous formation of chromium-rich corrosion products, which hinders the inhibitor adsorption.

From these observations, the occurrence of localized corrosion in inhibited 1Cr steel can be reasonably explained. Since the inhibitor is mainly anodic, it blocks the anodic areas more efficiently. Consequently, as film coverage increases, the relationship between anodic and cathodic areas decreases, so the corrosion rate

Table 3

Parameters from equivalent circuit modelling of impedance spectra of C–Mn steel in inhibited and uninhibited solution at 250, 1000, and 2500 rpm rotation rates.

C–Mn steel										
Exposure (h)	R_s (Ω cm ²)	Y_{CPEFO} (Ω^{-1} cm ⁻² s ⁿ 10 ⁻⁶)	n_{CPEFO}	R_{FO} (Ω cm ²)	Y_{CPEFI} (Ω^{-1} cm ⁻² s ⁿ 10 ⁻⁶)	n_{CPEFI}	R_{FI} (Ω cm ²)	Y_{CPEDL} (Ω^{-1} cm ⁻² s ⁿ 10 ⁻⁶)	n_{CPEDL}	R_{CT} (Ω cm ²)
250 rpm										
Uninhibited	6.1	–	–	–	–	–	–	693	0.81	131
Inhibited										
2	8.3	4.5	0.93	26	–	–	–	141	0.65	2831
24	8.4	4.1	0.93	346	21	0.67	11877	51	0.54	60549
1000 rpm										
Uninhibited	7.7	–	–	–	–	–	–	661	0.83	130
Inhibited										
2	5.4	2.7	0.94	304	29	0.55	14194	83	0.66	37308
24	9	1.8	0.96	579	9.4	0.62	80551	53	0.5	219600
2500 rpm										
Uninhibited	3.8	–	–	–	–	–	–	688	0.84	110
Inhibited										
2	4.1	2.6	0.93	1112	16	0.53	19911	46	0.52	48309
24	4.1	2	0.95	2432	6.5	0.65	83100	43	0.5	230438

Table 4

Parameters from equivalent circuit modelling of impedance spectra of 1Cr steel in inhibited and uninhibited solution at 250, 1000 and 2500 rpm rotation rates.

1Cr steel										
Exposure (h)	R_S ($\Omega \text{ cm}^2$)	Y_{CPEFO} ($\Omega^{-1} \text{ cm}^{-2} \text{ s}^n 10^{-6}$)	n_{CPEFO}	R_{FO} ($\Omega \text{ cm}^2$)	Y_{CPEFI} ($\Omega^{-1} \text{ cm}^{-2} \text{ s}^n 10^{-6}$)	n_{CPEFI}	R_{FI} ($\Omega \text{ cm}^2$)	Y_{CPEdI} ($\Omega^{-1} \text{ cm}^{-2} \text{ s}^n 10^{-6}$)	n_{CPEdI}	R_{CT} ($\Omega \text{ cm}^2$)
250 rpm										
Uninhibited	5.3	–	–	–	–	–	–	679	0.8	138
1000 rpm										
Uninhibited	6.2	–	–	–	–	–	–	680	0.82	132
Inhibited										
2	7.2	13	0.78	203	–	–	–	154	0.6	6095
24	12	2	0.86	265	32	0.54	1468	77	0.66	18242
2500 rpm										
Uninhibited	3.6	–	–	–	–	–	–	655	0.88	112
Inhibited										
2	3.2	4.9	0.86	338	–	–	–	125	0.61	9176
24	3.7	1.3	0.89	431	26	0.54	2695	53	0.65	33717

on the uncovered zones rises (as well as the local chromium concentration in corrosion products) yielding higher values than those found in the absence of the inhibitor. Once the chromium concentration of uncovered zones increases, the adsorption of the inhibitor becomes more difficult thereby preventing total area coverage and promoting the progress of the localized attack.

Under the particular flow rate conditions tested, inhibitor films are developed faster under higher rotation speeds for both steels. The enhancement in film formation kinetics would be related to the increase of the species mass transfer at the surface, which is proportional to rotation rate [28,29]. A greater surface mass transfer implies that more inhibitor molecules per unit of time are transported from the bulk of the solution to metal surface.

Similar results were found in other corrosion inhibitor studies [30,31]. This effect becomes critical for efficient inhibition of 1Cr steel, where it is necessary to accelerate the inhibitor film formation to cover the metal surface rapidly in order to decrease the accumulation of chromium-rich corrosion products.

In the case of C–Mn steel, increasing rotation rate improves short term inhibition (less than 2 h), since important differences in film coverage are observed. However, for longer term inhibition (24 h), the inhibitor efficiency yields practically the same value for all tested flow rates. This indicates that inhibitor film protection on C–Mn steel is satisfactory independently of surface mass transfer in the conditions tested.

Concerning the effect of flow-induced wall shear stress on inhibition, the experimental results indicate that applied shear stresses (approximately: 0.2, 1.8 and 8.7 Pa for 250, 1000 and 2500 rpm, respectively [28,29]) are not able to remove the formed inhibitor films.

The present results describe the performance of this type of inhibitor under simplified experimental conditions and a constricted time window (24 h). For these reasons, it is difficult to extrapolate the obtained data to predict the performance of 1% Cr steels in service. In any case, this information represents a warning and emphasizes the importance of steel chemical composition and hydrodynamic conditions in inhibitor selection tests.

5. Conclusions

- The imidazoline-based inhibitor used has a lower performance on carbon steel with 1% Cr. This behaviour can be attributed to the spontaneous formation of chromium-rich corrosion products, which hinder inhibitor adsorption.
- Inhibitor adsorption kinetics were enhanced with the increase of rotation rate on both carbon steels, with and without 1% Cr. This effect would be related to the increase of mass transfer, which promotes a greater availability of inhibitor molecules per unit of time from the bulk of the solution to metal surface.

- Fluid flow velocity may be an important parameter for the inhibition of carbon steel with 1% Cr. Effective uniform protection was achieved only at higher rotation rates where the inhibitor film covered the metal surface rapidly, decreasing the accumulation of chromium-rich corrosion products. For the lower rotation rate tested, localized corrosion was found.

Acknowledgements

This work was supported by CONICET (Argentine Research Council for Science and Technology) and ICMT (Institute for Corrosion and Multiphase Technology, Ohio University).

References

- [1] S.L. Fu, J.G. García, A. Griffin, NACE Corrosion 96, NACE International, Houston TX, USA, 1996, Paper 21.
- [2] S. Kapusta, S. Canter, NACE Corrosion 1994, NACE International, Houston TX, USA, 1994, Paper 10.
- [3] T. Rogne, T.G. Eggen, U. Steinsmo, NACE Corrosion 96, NACE International, Houston TX, USA, 1996, Paper 33.
- [4] M.M. Salama, B.N. Brown, NACE Corrosion 2009, NACE International, Houston TX, 2009, Paper 476.
- [5] H.J. Chen, Y. Chen, NACE Corrosion 2007, NACE International, Houston TX, 2007, Paper 623.
- [6] L.D. Paolinelli, T. Pérez, S.N. Simison, Mater. Chem. Phys. 126 (2011) 938–947.
- [7] S. Nestic, J. Postlethwaite, S. Olsen, Corrosion 52 (1996) 280–294.
- [8] R. Nyborg, NACE Corrosion 98, NACE International, Houston TX, 1998, Paper 48.
- [9] V. Jovancevic, S. Ramachandran, P. Prince, Corrosion 55 (1999) 449–455.
- [10] E. Gulbrandsen, J. Kvarekval, H. Miland, Corrosion 61 (2005) 1086–1097.
- [11] E. Gulbrandsen, A. Granå, Corrosion 63 (2007) 1009–1020.
- [12] M.B. Kermani, A. Morshed, Corrosion 59 (2003) 659–683.
- [13] C. de Waard, U. Lotz, A. Dugstad, NACE Corrosion 95, NACE International, Houston TX, USA, 1995, Paper 128.
- [14] A. Dugstad, H. Hemmer, M. Seiersten, NACE Corrosion 2000, NACE International, Houston TX, USA, 2000, Paper 24.
- [15] P.I. Nice, H. Takabe, M. Ueda, NACE Corrosion 2000, NACE International, Houston TX, USA, 2000, Paper 154.
- [16] M.B. Kermani, J.C. Gonzalez, C. Linne, M. Dougan, R. Cochrane, NACE Corrosion 2001, NACE International, Houston TX, 2001, Paper 65.
- [17] M.B. Kermani, J.C. Gonzalez, G.L. Turconi, D. Edmonds, G. Dicken, L. Scoppio, NACE Corrosion 2003, NACE International, Houston TX, USA, 2003, Paper 116.
- [18] M.B. Kermani, J.C. Gonzalez, G.L. Turconi, T. Perez, C. Morales, NACE Corrosion 2004, NACE International, Houston TX, USA, 2004, Paper 111.
- [19] K. Nose, T. Ishitsuka, H. Asahi, H. Tamehiro, in: EFC (Ed.), Advances in Corrosion Control and Materials in Oil and Gas Production (EFC 26), Maney Publishing, London, 1999.
- [20] ASTM Standard G0001-03, Standard Practice for Preparing, Cleaning, and Evaluating Corrosion Test Specimens, ASTM International, West Conshohocken PA, USA, 2003.
- [21] L.D. Paolinelli, T. Pérez, S.N. Simison, Corros. Sci. 50 (2008) 2456–2464.
- [22] C.H. Hsu, F. Mansfeld, Corrosion 57 (2001) 747–748.
- [23] D.A. López, S.N. Simison, S.R. de Sanchez, Corros. Sci. 47 (2005) 735–755.
- [24] V.S. Sastri, Corrosion Inhibitors. Principles and Applications, first ed. John Wiley & Sons, Chichester, 1998.
- [25] W. Durnie, Development of a Structure/activity Relationship for Carbon Dioxide Corrosion Inhibitors, Ph.D. Thesis, School of Applied Chemistry, Curtin University of Technology, 2000.

- [26] Y.J. Tan, S. Bailey, B. Kinsella, *Corros. Sci.* 38 (1996) 1545–1561.
- [27] M.E. Orazem, B. Tribollet, *Electrochemical Impedance Spectroscopy*, John Wiley & Sons, New Jersey, 2008.
- [28] D.C. Silverman, *Corrosion* 40 (1984) 220–226.
- [29] D.C. Silverman, *Corrosion* 44 (1988) 42–49.
- [30] M. Saremi, C. Dehghanian, M.M. Sabet, *Corros. Sci.* 48 (2006) 1404–1412.
- [31] P. Bommersbach, C. Alemany-Dumont, J.-P. Millet, B. Normand, *Electrochim. Acta* 51 (2006) 4011–4018.